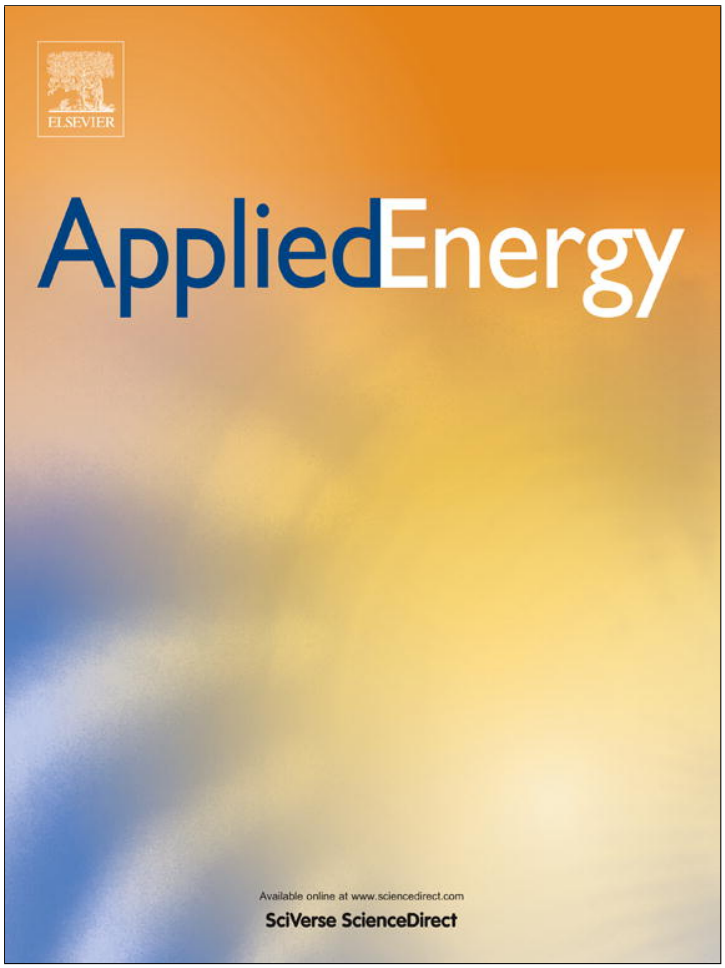

(This is a sample cover image for this issue. The actual cover is not yet available at this time.)

Applied Energy 107 (2013) 315–328

Contents lists available at SciVerse ScienceDirect

Applied Energy

journal homepage: www.elsevier.com/locate/apenergy

Exergy and economic analyses of advanced IGCC–CCS and IGFC–CCS power plants

Nicholas S. Siefert *, Shawn Litster

Mechanical Engineering Department, Carnegie Mellon University, United States

HIGHLIGHTS

- Exergy and economic analyses of two advanced fossil fuel power plants configurations.
- Adv. IGCC–CCS case includes H_2 and O_2 separation membranes and CO_2 capture.
- Adv. IGFC–CCS case includes catalytic gasifier, pressurized SOFC and CO_2 capture.
- Compared values of IRR and LCOE with conventional power plant configurations.
- Varied price of NG and CO_2 emissions to determine configuration with lowest LCOE.

ARTICLE INFO

Article history:
Received 13 September 2012
Received in revised form 8 January 2013
Accepted 2 February 2013

Keywords:
Fossil fuel
Coal gasification
Solid oxide fuel cell
Carbon capture and sequestration
Power plant economics

ABSTRACT

We present exergy and economic analyses of two advanced fossil fuel power plants configurations: an integrated gasification combined cycle with advanced H_2 and O_2 membrane separation including CO_2 sequestration (Adv. IGCC–CCS) and an integrated gasification fuel cell cycle with a catalytic gasifier and a pressurized solid oxide fuel cell including CO_2 sequestration (Adv. IGFC–CCS). The goal of the exergy analysis was to evaluate the power generation and the exergy destruction of each of the major components. We estimated the capital, labor, and fuel costs of these power plants, and then calculated the internal rate of return on investment (IRR) and the levelized cost of electricity (LCOE). In the Adv. IGFC–CCS case, we chose a configuration with anode gas recycle back to the gasifier, and then varied the SOFC pressure to find the optimal pressure under this particular configuration. Using a base load generation price of electricity of \$50/MWh, the IRR of the Adv. IGFC–CCS configuration was 4 ± 3%/yr if the CO_2 can be used for EOR and 1 ± 3%/yr if the CO_2 can only be sequestered in a saline aquifer. The IRR of the Adv. IGCC–CCS configuration with H_2 and O_2 membrane separation was 8 ± 4%/yr if the CO_2 can be used for enhanced oil recovery (EOR) and 3 ± 3%/yr if the CO_2 must be sequestered in a saline aquifer. The uncertainty here reflects the uncertainty in capital costs, operation & maintenance (O&M) costs, and CO_2 sequestration costs.

One goal of the economic analysis was to compare the IRR and LCOE of these configurations with the IRR and LCOE of other fossil fuel power plant configurations. For example, using capital/labor/maintenance cost estimates from the literature, we calculated the IRR and LCOE of conventional fossil fuel power plant configurations, including scenarios with CCS and scenarios with varying costs to emit CO_2. We also present results on which power plant configuration yields the lowest value of LCOE as a function of the price of CO_2 emissions and a function of the price of natural gas, holding all other variables constant. An Adv. IGCC–CCS–EOR configuration yields the lowest value of LCOE when the price of natural gas and the price of CO_2 emissions are above the line between (\$5/GJ, \$10/tCO_2) and (\$2.5/GJ, \$50/tCO_2).

Published by Elsevier Ltd.

1. Introduction

Pulverized coal combustion (PCC) power plants generate between 40% and 50% of the total supply of electricity in the United States [1]. However, this percentage is likely to decrease in the future because of the currently low price of natural gas as well as the recent proposed regulations on the emission of greenhouse gases by the Environmental Protection Agency [2]. While the future for building new PCC power plants looks bleak, the future may not be as bleak for building advanced integrated gasification combined cycle with carbon capture and sequestration (IGCC–CCS) and

* Corresponding author.
E-mail address: nsiefert@andrew.cmu.edu (N.S. Siefert).

0306-2619/$ - see front matter Published by Elsevier Ltd.
http://dx.doi.org/10.1016/j.apenergy.2013.02.006

advanced integrated gasification fuel cell with carbon capture and sequestration (IGFC–CCS) power plants that operate off of mixtures of coal, municipal solid waste, or petroleum coke.

Herzog [3] published in 1999 one of the first reports detailing the economic costs of carbon dioxide capture at coal power plants. Since then, there have been a number of economic analyses of advance fossil power plants with and without carbon dioxide capture, such as Johnson and Keith [4], Rubin et al. [5,6], Davison [7], Patino-Echeverri et al. [8], Kunze and Spliethoff [9], Hu et al. [10], Hammond et al. [11], Fischbeck et al. [12], Viebahn et al. [13], Pettinau et al. [14] and Melchior and Madlener [15]. Johnson et al. [4] and Fischbeck et al. [12] have analyzed the effect of both natural gas prices and the price of carbon dioxide emissions on the economic viability of the various fossil fuel power plant configurations. There have also been numerous studies on the economic viability of various fossil fuel power plants configuration conducted by the National Energy Technology Laboratory (NETL) and the Energy Information Administration (EIA). Some recent NETL studies on the economics of various advanced coal power plants with CCS, such as by Gerdes et al. [16,17] and Grol and Wimer [18], include capital cost estimates of advanced IGFC–CCS power plant configurations. The Adv. IGCC–CCS and Adv. IGFC–CCS configurations analyzed here are similar to the configurations modeled by Gerdes et al. [16,17] and Li et al. [19], with the main difference being that Li et al. [19] included the sale of both electricity and hydrogen.

Herein, we present our exergy and economic analyses of two different advanced gasification based power plants where the main product was electricity. The first configuration analyzed is similar to a conventional IGCC–CCS configuration [16,20], but with a few noticeable changes: (1) ion transport membranes (ITMs) for O_2 separation rather than cryogenic air separation; (2) warm gas sulfur removal with alkali hydroxide rather than low temperature removal using physical solvents; and (3) palladium membranes for H_2 separation from the syngas rather than low temperature removal of CO_2 from the syngas using physical solvents. The second configuration analyzed is an advanced IGFC–CCS configuration in which a catalytic coal gasifier is coupled with a pressurized hybrid solid oxide fuel cell featuring a compressor and turbine pair that can operate at pressures between 0.2 and 0.8 MPa. For both configurations, we calculated the exergy efficiency, the internal rate of return on investment (IRR), and the levelized cost of electricity (LCOE). We then compared the values of IRR and LCOE to other fossil fuel power plants. The goal of the exergy analysis in this paper was not to optimize the power plant for exergy efficiency, but rather was to determine where in the power plant exergy is lost due to irreversible processes.

In addition to conducting exergy and economic analyses of these particular configurations, we compare the cost of electricity of these two advanced power plants with power plant configurations designed to meet potential Environmental Protection Agency (EPA) regulations that limit greenhouse gas emissions from new large-scale power plants to less than 0.45 kg (1 lb) of CO_2 per kW h of electricity generated. To meet these proposed requirements, a PCC or an IGCC power plant needs to capture and sequester roughly 50% of the carbon dioxide produced at the power plant. We label these power plant configurations PCC–50%CCS and IGCC–50%CCS. In this paper, we compare the IRR and LCOE calculated in this report to the IRR and LCOE of other power plant configurations analyzed by Rubin et al. [5] and Gerdes et al. [16,17]. In addition, we analyze at what price of natural gas and at what price of CO_2 emissions can advanced coal based power plants with CCS compete economically with natural gas combined cycle power plants (NGCCs).

2. System and exergy analysis

Exergy and thermo-economic analyses date back to at least the 1960s [21], and have been reviewed by El-Sayed [22]. Exergy is not a standard thermodynamic variable because the exergy of a system is given with respect to the temperature, pressure and composition of the Earth's atmosphere, which is not the same at different times or locations. Our assumed standard state is the following: 25 °C, 0.10 MPa, and a molar gas composition of 78% N_2, 20% O_2, 2% H_2O, and 0.04% CO_2. The exergy of a system is the maximum useful work that can be generated during a process that brings the system into thermal, chemical and mechanical equilibrium with the system's environment. Exergy can exist in multiple forms, such as thermo-mechanical exergy and chemical exergy; there are also corresponding forms of exergy for kinetic, potential, and electrical energy. If ignoring the potential and kinetic exergy of the flow, the molar exergy of a substance flowing into or out of a control volume can be defined as:

$$\hat{\varepsilon} = (\hat{h} - \hat{h}_0) - T_0(\hat{s} - \hat{s}_0) + \Sigma_i x_i(\hat{\mu}_i - \hat{\mu}_{i_0}) \tag{1}$$

where $\hat{h}$ is the molar enthalpy, T is the temperature, $\hat{s}$ is the molar entropy, x_i is the mole fraction of species i, and $\hat{\mu}_i$ is the chemical potential of species i at standard temperature and pressure. Terms without the naught symbol are for the system, and terms with the naught symbol are for the environment. The exergy of a substance cannot be negative, and it is only equal to zero when the substance is in thermal, chemical and mechanical equilibrium with its environment. By combining the first and second laws of thermodynamics for open, steady-state processes, one obtains the exergy balance equation:

$$\dot{W}_{useful} = \Sigma_i \dot{n}_i \hat{e} + \Sigma_k \left(\frac{T_k - T_0}{T_k}\right)\dot{Q}_k - T_0 \cdot \dot{\sigma}_{irr} \tag{2}$$

where $\dot{W}_{useful}$ is the amount of useful mechanical and electrical work generated from the system, $\dot{n}_i$ is the molar flow rate into or out of the control volume of component i, T_k is the temperature at which heat $\dot{Q}_k$ flows out of or into the control volume, T_0 is the reference temperature of the environment, and $\dot{\sigma}_{irr}$ is the rate of entropy generation inside of the control volume due to irreversible processes. It is these irreversible processes, such as the flow of particles across gradients in temperature, pressure or chemical composition, which cause exergy destruction. When exergy is destroyed, there is a loss in the amount of useful work available that can be generated from the original exergy available to the system. The amount of exergy destruction is given by the Gouy–Stodola theorem [23]:

$$\Phi_{des} = T_0 \cdot \sigma_{irr} \tag{3}$$

where Φ_{des} is the exergy destruction and σ_{irr} is the amount of entropy generated by irreversible processes. Some of the value in conducting an exergy or second law analysis, in addition to a first law analysis, are the following: (1) identification of how much potentially useful work is destroyed within processes within the plant, (2) ensuring that none of the individual idealized processes inside of the plant violate the second law of thermodynamics, and (3) ensuring that the total exergy entering the plant is equal exactly to the amount of exergy leaving the plant plus the exergy destruction inside of the plant. While a standard exergy analysis is an important check to understand where improvements in the plant might be possible, a standard exergy analysis does not include calculations of the cost and/or exergy destruction associated with building and maintaining the power plant. Therefore, while an exergy analysis is useful in estimating the cost to fuel the power plant, an exergy analysis is not a substitute for a full economic analysis of a particular power plant configuration.

2.1. Adv. IGCC with H_2 and O_2 separation membranes

2.1.1. Description of process flow diagram

We conducted an exergy analysis of an integrated gasification coal power plant with advanced hydrogen and oxygen separation membranes. Mass and energy balances for each of the individual reactors in the system were conducted using HSC Chemistry 6.0 (Outotec, Espoo, Finland), which also calculated the chemical equilibrium composition given input flows by minimizing the Gibbs free energy. Mass, energy and exergy balances were conducted using Cantera v1.7, which is open source software by D.G. Goodwin. Fig. 1 shows the process flow diagram for all the flows and equipment modeled for this configuration. The following sub-sections provide a description of the technologies used in the process and highlight some important technological details.

2.1.1.1. Gasification. We modeled a GE entrained flow gasifier using HSC Chemistry. Coal is crushed and then mixed with water before entering a slurry pump to pressurize the slurry to 4.2 MPa. The temperature at the exit of the gasifier is 1200 °C, but after the syngas cooler, the temperature is 860 °C. We used a H_2O-to-carbon ratio and an O_2-to-carbon ratio in the gasifier of 0.46:1 for both H_2O and O_2, which generates a syngas composition of 30% H_2, 48% CO, 15% H_2O, and 7% CO_2 using Gibbs free energy minimization in HSC Chemistry.

2.1.1.2. Syngas quench, sulfur removal and water gas shift. After exiting the syngas cooler, the syngas is quenched with liquid water containing sodium hydroxide. The sodium hydroxide is used to capture acid gases, such as hydrogen sulfide and carbonyl sulfide. We assumed the presence of 0.5% molar composition of H_2S plus COS in the syngas for the economic model. We assume that the hydrogen sulfide and carbonyl sulfide is converted into elemental sulfur via either the Thiopaq (Paqell, Balk, The Netherlands) and LO-CAT (Merichem, Houston, TX) processes.

After exiting the quench reactor, the syngas is saturated with water at a temperature of 250 °C, and then is sent to a bed of activated carbon to remove mercury and to remove any further H_2S in the gas stream. The syngas then enters a water gas shift (WGS) reactor at a constant temperature of 250 °C and a constant pressure of 4.2 MPa. The syngas composition exiting the WGS reactor is 54% H_2, 3% CO, 7% H_2O, and 37% CO_2, using Gibbs free energy minimization constrained to not form methane in the reactor. The thermal energy from the WGS reactor is removed via heat transfer with steam in the Rankine cycle.

2.1.1.3. Hydrogen separation. There are various methods of separating hydrogen from syngas streams using inorganic membranes [24]. This technology is still in the early stages of commercial development. Typically, palladium is used because of its high permeability for hydrogen diffusion through the solid. The palladium is normally doped with other metals, such as copper, in order to reduce the cost of the membrane and to increase the tolerance of the alloy to hydrogen sulfide poisoning [25,26]. The flux through the membrane was estimated using data from prior research on palladium alloy membranes [27] chosen at the temperature after the syngas compressor of 726 K. The hydrogen pressure on the pure side of the membrane is assumed to be to be 0.5 MPa, yielding a normalized flux of hydrogen through the membranes of roughly 0.02 mol m^{-2} s^{-1}.

2.1.1.4. Carbon dioxide capture. The hydrogen-depleted stream from the palladium membrane reactor is oxy-combusted with just enough oxygen to convert all carbon monoxide into carbon dioxide and all remaining hydrogen into water vapor. After catalytic

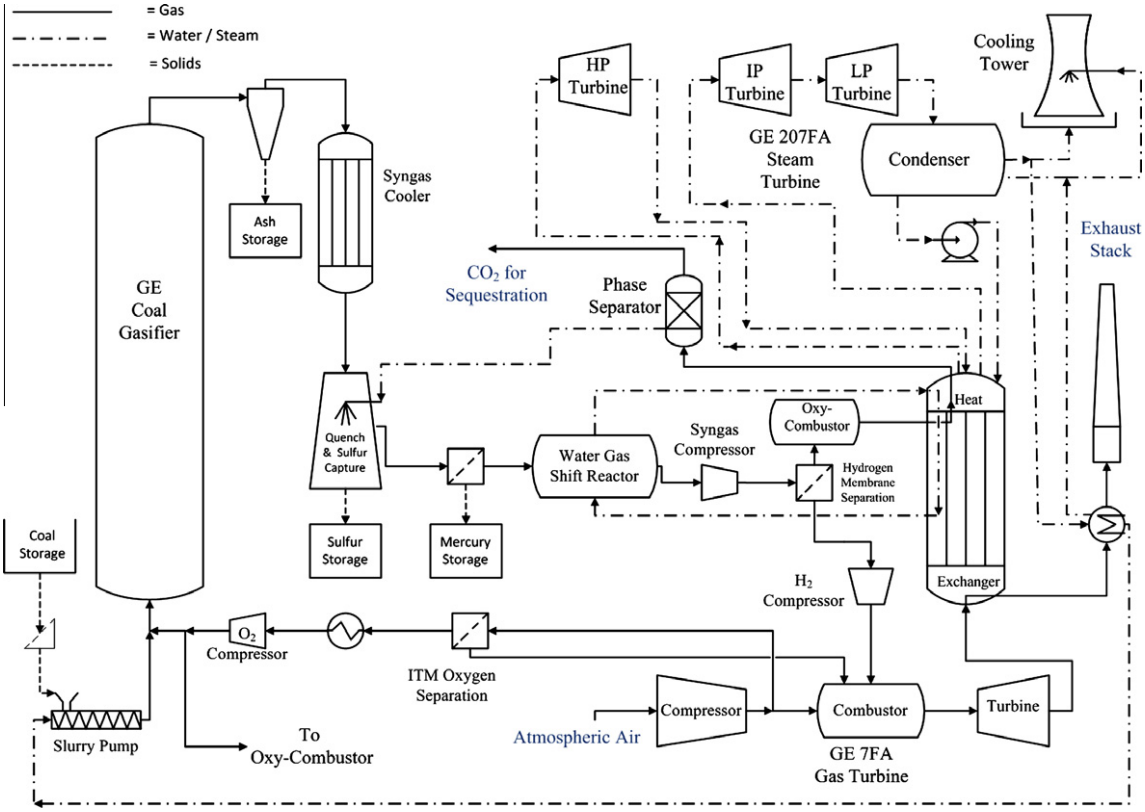

Fig. 1. Process flow diagram of the IGCC–CCS process modeled. *Left*: coal gasification and quench, *Middle*: water gas shift and H_2 separation, *Bottom*: Brayton cycle and O_2 separation, and *Top Right*: Rankine cycle.

Table 1
System output variables for the Adv. IGCC–CCS configuration model in this report.

Brayton cycle power output	511 MW
Rankine cycle power output	459 MW
Total power output	808 MW
Coal input rate	5230 ton/day
CO_2 produced	14,640 ton/day
CO_2 capture rate	14,640 ton/day
Thermal efficiency (HHV)	43.4%
Exergetic efficiency	42.8%

oxy-combustion so that there is no oxygen remaining in the gas stream, the gases are cooled such that they leave the heat exchanger as liquid water and supercritical carbon dioxide. The carbon dioxide is separated and pumped to an existing CO_2 pipeline that is assumed to be located 50 km from the power plant.

2.1.1.5. ITM oxygen separation. In order to increase the system efficiency and decrease the capital cost compared to an IGCC–CCS configuration with cryogenic air separation, Air Products and Chemicals, Inc. (Allentown, PA) is currently developing ion transport membranes (ITMs) to provide the oxygen for the gasifier [28]. In this Adv. IGCC–CCS configuration, oxygen is separated for use throughout the process by sending the hot, compressed gas from the exit of a Brayton cycle compressor to the ITM separation reactor. We assume that the mixed ionic–electronic ceramics of the ITM are 100% selective in separating oxygen from air. This process requires temperatures between 800 °C and 900 °C, and a sizeable pressure difference [29], yielding a normalized flux of oxygen of roughly 0.03 mol m^{-2} s^{-1}. The pressure on the air side of the membrane is the same as the pressure of the Brayton cycle turbine (1.7 MPa). We assume that the pressure of oxygen on the pure oxygen side of the membrane is 0.1 MPa, and therefore, the oxygen must be cooled and compressed to 4.2 MPa before entering the gasifier and compressed to 15.0 MPa before entering the oxy-combustor.

2.1.1.6. Brayton cycle. The Brayton cycle turbine modeled here is the GE 9001FA model with a power output of 255.6 MW, a pressure ratio of 17.0 and a heat rate of 9757 kJ per kW h. The model assumes the plant operates two of these turbines for a total Brayton cycle power output of 511 MW. Using this publically available data on the GE 9001FA, we calculated that the isentropic efficiency of the compressor and turbine of the Brayton cycle was 86%. In the combustor, hydrogen reacts with air from the main compressor and with the depleted air from the ITM oxygen separation process. The pure hydrogen stream leaving the palladium membranes is compressed from 0.5 MPa to the pressure of the Brayton turbine combustor (1.7 MPa). The main system compressor provides approximately 235% excess air. This limits the adiabatic flame temperature of the combustor to 1430 °C, the specified firing temperature for the turbine. The combusted gases pass through the vanes of the turbine and are then sent to the steam generator for the Rankine cycle.

2.1.1.7. Rankine cycle. The main Rankine steam generator utilizes the thermal energy from the Brayton cycle exhaust, the thermal energy from the carbon capture oxy-combustion exhaust, the thermal energy from the water gas shift reactor, and the thermal energy obtained by cooling the pure oxygen stream before the gasifier. This thermal energy is used to generate the steam necessary to drive the high-pressure (HP) steam turbine. The HP turbine exhaust is sent through a portion of the steam generator to provide the reheat necessary for the intermediate pressure (IP) turbine. The exhaust of this turbine is sent directly through the low-pressure (LP) turbine. Here, we consider a GE 207FA steam turbine with a HP stage at 13 MPa/565 °C, an IP stage at 3 MPa/565 °C, and an LP stage at 0.5 MPa with no reheat. We assumed an isentropic efficiency of 90% when modeling the Rankine cycle. The three stages have a total output of 459 MW.

2.1.2. Technical performance

As seen in Table 1, the total power output was calculated to be 808 MW. This accounts for electricity generated by the two gas turbines as well as the Rankine cycle steam turbine. It also includes plant electricity requirements for all major system loads present in the process diagram in Fig. 1. Using the assumptions listed above, the power plant operates at a HHV thermal efficiency and exergetic efficiency of around 43%. For comparison, NETL's analysis of an IGCC–CCS power plant with ITM, H_2 Sep & G9FA is quite

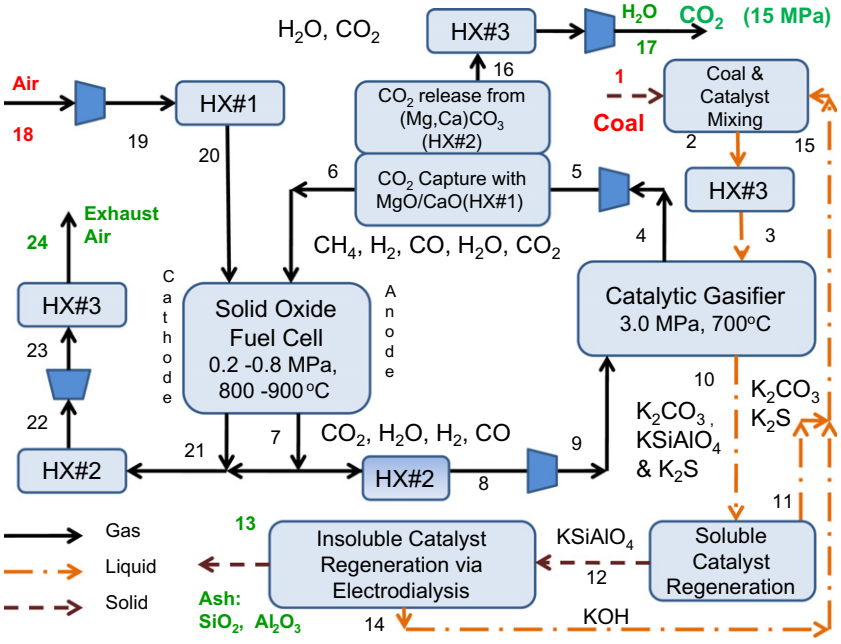

Fig. 2. Process flow diagram for catalytic steam gasification integrated with a SOFC.

Table 2
Exergy destruction and exergy output as a percentage of the inlet exergy for an Adv. IGCC–CCS configuration with H_2 and O_2 membrane separation.

Net power exiting	42.8%
Gasifier RC HX	19.6%
Brayton cycle combustor	12.4%
SC CO2 exiting	6.2%
Steam turbine	4.2%
WGS reactor and RC HX	2.9%
Brayton cycle turbine	2.9%
Post-brayton cycle HX	2.1%
Syngas quench	2.0%
Rankine cycle condenser	1.4%
H_2 membrane + H_2 compressor	1.4%
Brayton cycle compressor	0.9%
Exhaust air	0.9%
O_2 membrane	0.2%
Rankine Cycle Pump	0.1%
Sum	100.0%

similar to the flow diagram studied here [16], in which they measured a HHV efficiency of 40% as seen in Fig. 3, which will be discussed further in section 2.3.

2.1.3. Exergy analysis

In this section, we analyze each of the main locations of exergy destruction (irreversible entropy generation) within the power plant. Table 2 shows a list of sources for the exergy destruction, as well as the amount of exergy leaving the power plant, normalized by the inlet exergy flow of the incoming coal. We calculated that 42.8% of the inlet exergy will leave the system as electricity, 6.2% will leave as exergy in the compressed carbon dioxide, and only 0.9% will leave as the exhaust's thermal exergy. The largest sources of exergy destruction are the coal gasifier/syngas cooler section (19.6%), the combustor of the Brayton cycle (12.4%), the steam turbine (4.2%), the gas turbine (2.9%), WGS reactor with associated heat exchanger (HX) (2.9%), Post-Brayton Cycle HX (2.1%), the quench system (2.0%), the H_2 membrane separation process (1.4%), the gas compressor (0.9%), the ITM O_2 separation membrane reactor (0.2%), and finally the Rankine Cycle Pump (0.1%). The exergy destruction in the gasifier was significant because there is an inherent mismatch between the temperature of gasification (1200 °C) and the temperature at which the heat is transferred to the steam in the Rankine cycle (<600 °C). There was also significant exergy destruction in the combustor because, even though the temperature of the combustor is quite high, this is the location where most of the fuel is oxidized.

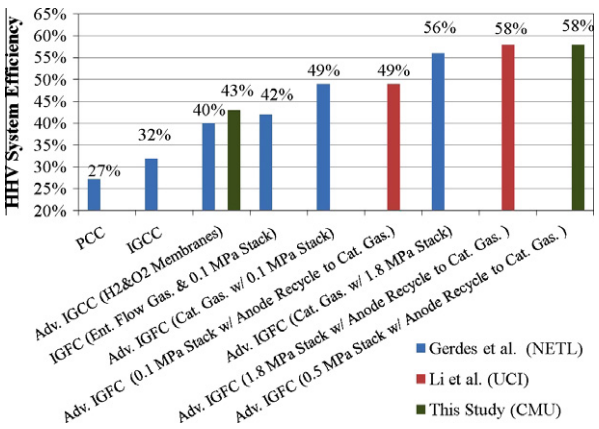

Fig. 3. First law system efficiency for various power plant configurations with greater than 90% CO_2 capture and compression to 15 MPa.

2.2. Adv. IGFC with catalytic gasifier and pressurized SOFC

2.2.1. Description of process flow diagram

We conducted an exergy analysis of a power plant design in which a catalytic coal gasifier produces a methane rich syngas. Carbon dioxide is captured from the syngas before the syngas is sent to a SOFC. In this design, the anode tail gas from the SOFC is recycled back to the catalytic gasifier. Fig. 2 shows the process flow diagram for the major components of this system. We used HSC Chemistry for both a first law balance and a material balance for the catalytic gasifier, the CO_2 capture/release reactors, and the SOFC. The gas compositions throughout the loop of Steps 4–9 are listed in Table 3 when the single pass utilization of the SOFC was 70%. Since this is a process with a recycle loop and with multiple species capable of being oxidized in the fuel cell, 'single pass fuel utilization' is defined to be equal to the amount of oxygen that crosses from the cathode to the anode divided by the amount of oxygen that would cross from the cathode to the anode if all of the H_2, CO, and CH_4 entering the anode were completely oxidized to H_2O and CO_2.

2.2.1.1. Catalytic coal gasifier. The catalytic gasifier modeled here is based off of the Exxon single-stage, fluidized bed catalytic gasifier [30,31], in which low rank coals are slurry mixed with roughly 20 wt.% potassium hydroxide and carbonate. A slurry of coal, catalyst and water is pumped to the pressure of the gasifier (3 MPa) and then dried using exhaust air from the low pressure Brayton cycle. This catalytic gasifier operates adiabatically at a temperature of 700 °C. The dried coal and catalyst enter the catalytic gasifier along with the anode gas recycle from the SOFC. The gasifier is operated adiabatically. The molar methane composition of the syngas from the catalytic gasifier is roughly 20% on a dry basis [30,31], because of non-equilibrium effects such as methane volatilization from coal [32], but these effects could not be modeled in a chemical simulator that minimizes the Gibbs free energy. In addition to catalyzing the steam–coal gasification reaction, the alkali catalyst also can capture acid gases, such as hydrogen sulfide [33], which simplifies the syngas cleanup steps before the SOFC.

2.2.1.2. Catalyst regeneration. The catalyst, ash and unconsumed carbon exit the gasifier and are quenched with water. We assume that the residence time in the gasifier is such that there is only 1% unconsumed carbon compared with the initial energy content of the coal. After the catalyst, ash and unconsumed carbon are quenched with water, and soluble species will enter the aqueous phase, such as potassium carbonate, potassium sulfide and some potassium alumina-silicate species. Yeboah et al. [34] and Sheth et al. [35] have studied the effect of different catalysts on the gasification rate, and determined that when the potassium is bonded to weak anions (such as OH^-, S^{2-} and CO_3^{2-}), the kinetics rates of gasification were higher than when bonded to strong anions (such as Cl^-) that are stable in gasification environments. Since potassium carbonate and potassium sulfide are both water soluble and active catalysts, the water soluble catalysts can be recovered at this stage and mixed with fresh coal.

When alkali cations react with alumina-silicates in the coal ash, their ability to catalyze steam–coal reactions significantly decreases [36]. Since alkali cations thermodynamically prefer being chemically bonded to alumina-silicates than being bonded with carbonate anions or sulfide anions, the alkali cations must be recovered from alkali alumina-silicates in order to maintain the catalytic capability of the alkali ions.

$$H_2O(l) + K_2Al_xSi_yO_z(s) = Al_xSi_yO_z(s) + 2KOH(a)$$
$$\Delta G^{300K} \approx +12\ \text{kJ/mol} \quad (4)$$

Table 3
Syngas composition throughout the loop that integrates the catalytic gasifier with the SOFC, as calculated by HSC Chemistry using Gibbs free energy minimization, when the single-pass fuel utilization was 70%.

	Gasifier exit (4) (%)	Post CO_2 capture (6) (%)	Post SOFC anode (7) (%)
H_2	32	58	29
CO	13	2	6
CO_2	13	1	6
H_2O	34	15	59
CH_4	8	14	0

To determine the amount of electricity required to generate alkali hydroxides from the alumina-silicates, we first calculated the amount of alkali species that react with alumina-silicates in the gasifier based on the ash content of the coal. For this configuration, we assume that the coal is a low ash, low sulfur coal from Power River Basin, WY with a weight fraction of 0.5% kg kg^{-1} sulfur and 5% kg kg^{-1} alumina-silicate. We then estimate the amount of electricity consumption by multiplying the molar flow of alkali alumina-silicates times the ΔG of Eq. (4), and then divide this quantity by an electrodialysis electrical efficiency of 40%. We chose the value of 40% because it falls within the range of the electrodialysis efficiencies measured experimentally by Nagasawa et al. [37].

As stated earlier, the actual consumption of electricity in the electrodialysis unit will depend on the ash content of the coal. As will be shown in the exergy analysis section, catalyst regeneration using bipolar membrane electrodialysis consumes roughly 1% of the gross electricity generated at the power plant if a low ash coal is used as fuel and if the weight of the alkali carbonate catalyst is 0.2 kg for every 0.8 kg of coal used.

2.2.1.3. Carbon dioxide capture. There are various methods of removing carbon dioxide from coal gasification syngas [38]. Commercially available physical solvents, such as Selexol (UOP LLC) or Rectisol (Linde AG and Lurgi AG), require lowering the temperature to below the dew point of the syngas. Instead, we model a chemical capture process that leaves the temperature of the syngas close to the inlet temperature of the solid oxide fuel cell. After leaving the catalytic gasifier, the methane rich syngas goes through an expander to drop the pressure of the gas to the pressure of the SOFC. Then the gas goes to a reactor filled with magnesium and calcium oxide (MgO, CaO) in order to capture CO_2 as well as any remaining H_2S and COS in the gas stream [39]. Carbon dioxide capture occurs at a temperature of 750 °C or less, depending on the pressure after the expander. The CO_2 is regenerated from the dolomite ($MgCO_3$, $CaCO_3$) using hot exhaust gases from the SOFC at a temperature of 1000 °C and a pressure of 0.1 MPa. After this, the carbon dioxide is cooled, compressed, cooled, dried, and then compressed to a pressure of 15 MPa for subsequent injection into a carbon dioxide pipeline.

2.2.1.4. SOFC. The syngas leaving the CO_2 capture reactor then enters the anode of the SOFC. The SOFC is the main source of electricity generation from this power plant configuration. The SOFC is modeled using *V–i* curves at various SOFC temperatures and pressures using publically-available data from Rolls Royce Fuel Cell Systems [40]. The equation used to model the fuel cell voltage was the following:

$$V = \frac{-g_{f,\mathrm{H2O(g)}}(T, 1\ \mathrm{atm})}{2F} + \frac{RT}{2F}\ln\left[\frac{p^{\mathrm{anode}}_{\mathrm{H2(g)}} \cdot \left(p^{\mathrm{cathode}}_{\mathrm{O2(g)}}\right)^{1/2}}{p^{\mathrm{anode}}_{\mathrm{H2O(g)}}}\right] - i \cdot ASR - \frac{RT}{(\alpha z)\cdot F}\ln\left(\frac{i}{i^0_o}+1\right) \quad (5)$$

The voltage, *V*, between the anode and the cathode is equal to the open circuit voltage minus the Ohmic overpotential minus the electrode overpotential, where *i* is the operating current density in [A cm^{-2}] and (αz) is the transfer coefficient, which we assume to be equal to a value of 2 in order to estimate the electrode exchange current density, i^0_o. The Gibbs free energy of formation of water from H_2 and O_2 as function of temperature at 1 atm, $g_{f,\mathrm{H2O(g)}}$ (T, 1 atm), was determined using HSC Chemistry. The pressures are the average pressure along the length of the fuel cell and the units of pressure in the equation above are atmospheres. The values of the Ohmic area specific resistance, *ASR*, and the electrode exchange current density, i^0_o, are both functions of temperature, and the electrode exchange current density is also a function of pressure. We determined the values of *ASR* and i^0_o by fitting publically available data from Rolls Royce Fuel Cell Systems [40]. Since the Rolls Royce data was given as both a function of temperature and pressure, we were able to calculate the following values of *ASR* and i^0_o.

$$ASR\ [\Omega\ \mathrm{cm}^2] = 0.12 + 0.18 \cdot e^{6500\cdot\left(\frac{1}{T}-\frac{1}{1123}\right)}. \quad (6)$$

$$i^0_o\ [\mathrm{A}\cdot\mathrm{cm}^2] = 0.01 \cdot p[\mathrm{atm}] \cdot e^{6500\cdot\left(\frac{1}{T}-\frac{1}{1123}\right)} \quad (7)$$

where T is the temperature in Kelvin. Using this empirically fit data, we were able to calculate the voltage of the fuel cell as a function of temperature, pressure and gas composition.

After leaving the fuel cell, as seen in Fig. 2, most of the anode tail gas goes directly to HX2; however, a small portion of the tail gas is mixed with the depleted air exiting the cathode. This is effectively a bleed stream in order to prevent the build of inert gas species, such as N_2 in originally in the coal as nitrogen species, and to prevent the buildup of water vapor.

Gaseous fuels like methane, ammonia and carbon monoxide are internally reformed or shifted in the anode channels of the SOFC to yield the hydrogen that reacts with oxygen ions on the anode [41,42]. There have been a number of research groups that have demonstrated experimentally the capability of doped Ni–YSZ anodes to reform methane and higher hydrocarbons [43–49]. For example, Shiratori et al. [46] experimentally demonstrated operation of a SOFC for 50 h with direct biogas using a Ni–ScSZ cermet as the anode material. While most anodes composed of pure Ni–YSZ are not tolerant to high levels of H_2S or to hydrocarbons, Yang et al. [48] showed that Ni–YSZ anodes doped with barium and cerium are more tolerant to both hydrogen sulfide and propane.

2.2.1.5. Brayton cycle. Depending on the fuel cell pressure, there can be significant net power generation from the combined air compressor and exhaust turbine. In this configuration, the air is first compressed and then sent to the CO_2 capture reactor to provide the cooling required to maintain the temperature for CO_2 capture below 750 °C. The air then enters the cathode of the fuel cell. After the cathode, the air combines with the portion of the anode tail gas that is not recycled back to the catalytic gasifier. This exhaust gas is combusted, raising the temperature of the exhaust to the point at which it can be heat exchanged with the magnesium and calcium carbonate exiting the CO_2 capture reactor. After HX#2, the exhaust air passes through an exhaust turbine. The isentropic efficiency of all compressors and turbines in this system was assumed to be 80%.

2.2.2. Exergy analysis

We now focus on the exergy analysis on this configuration that integrates a catalytic gasifier with a pressurized fuel cell operating on a methane-rich syngas. We calculated an exergetic efficiency of 58.3% for the operating conditions listed in Table 4: catalytic

gasifier pressure was 3.0 MPa; SOFC pressure was 0.5 MPa; air stoichiometric ratio was 2.0; SOFC current density was 0.5 A cm^{-2}; SOFC Voltage was 0.70 V; and SOFC single pass fuel utilization was 70%. In Table 4, we list where power is either generated or consumed as well as where exergy is destroyed in the power plant due to irreversible processes. Our calculations in Table 4, as well as those by Li et al. [50], show that the system efficiency for power plants with catalytic gasification with anode recycle is near 60%.

As seen in Table 4, the largest source of exergy destruction was the CO_2 capture using a combination of calcium and magnesium oxide and the associated heat exchangers to cool or heat the solid materials. The second largest source of exergy destruction was the SOFC. The exergy destruction inside the SOFC is due to irreversible processes within the fuel cells, principally Ohmic and cathode activation losses. Using the Gouy–Stodola Theorem as presented in Eq. (3), the exergy destruction of a methane-fueled SOFC at constant temperature is roughly equal to the overvoltage, η, times the current times the temperature of the environment (298 K), T_o, divided by the temperature of the SOFC, T_{SOFC}, and divided by the exergy of the fuel into the power plant normalized by the fuel's reduction charge [33].

$$\text{SOFC exergy destruction}[\%] \cong \frac{\eta}{1\,\text{V}} \cdot \frac{T_0}{T_{\text{SOFC}}} \tag{8}$$

Depending on the fuel, the exergy divided by the reduction charge, i.e. the number of electrons generated if the fuel is fully oxidized on an electrode, is typically between 1.0 and 1.3 V. Given the amount of electricity generated in the SOFC, the SOFC is not a major source of exergy destruction because the temperature of the SOFC is nearly four times larger than the temperature of the environment.

The third largest source of exergy loss is the 150 bar CO_2 leaving the power plant. This high pressure is required to overcome friction in the pipeline and to overcome the pressure of a typical geologic reservoir. Here, we count the exergy required to sequester the CO_2 as exergy destruction because the pressurized carbon dioxide is not being used to generate electricity at the power plant, even though this mechanical form of exergy is used for useful purposes in the EOR case. There was only minor exergy destruction inside of the catalytic gasifier because there is no oxygen consumption inside of the catalytic gasifier. The exergy destruction of the turbines and compressors were each 3% or less.

2.3. Comparison with other researchers

It has been shown by Gerdes et al. [16,17], Grol and Wimer [18], Shelton et al. [51], and Li et al. [50] that coal-based power plants using catalytic gasifiers and pressurized fuel cells can achieve system efficiencies of ~60% while sequestering >90% of the carbon dioxide generated at the power plant. Though, there are some notable differences in the approaches in each of the studies listed above. A few key differences between the Adv. IGFC system analyzed here and some of the Adv. IGFC systems analyzed by previous research are: (a) anode tail gas recycle back to the gasifier; (b) CO_2 capture before the SOFC; (c) no steam turbine; and (d) intermediate SOFC pressure. The SOFC pressure in other system analyses has either been 0.1 MPa or greater than 1 MPa. Here, we analyzed cases between 0.2 MPa and 0.8 MPa. We chose to capture CO_2 before the SOFC because this CO_2 capture step will reduce the chance of carbon build-up on the anode electrode and also remove the majority of any remaining sulfur species in the syngas. Since IGFC system designs vary significantly between research groups, the optimal configuration depends on the exact constraints and costs of fuel cell systems. Also, since many of the main pieces of equipment in an IGFC power plants are not commercial-off-the-shelf technology and since their performance and cost are still evolving, there is no way to definitely prove that there is an optimal configuration.

Table 4
Exergy balance for a SOFC operating on syngas from a catalytic gasifier and anode tail gas recycle back to the catalytic gasifier. Pressure of the SOFC was 0.5 MPa; air stoichiometric ratio was 2.0; SOFC current density was 0.5 A cm^{-2}; SOFC voltage was 0.7 V; and SOFC temperature was 1123 K (850 °C).

Process step	Power/inlet exergy (%)	Exergy destruction or loss/inlet exergy (%)
Air compressor (18–19)	−12.9	0.8
Air turbine (22–23)	+13.8	1.1
Exhaust air (24)	+0.8	2.3
CO_2 compressor (16–17)	−1.4	0.4
Exhaust CO_2 (17)	–	5.5
CO_2 capture HX's (5, 6, 7, 8, 19, 20, 21, 22)	–	12.9
Catalyst regeneration with electrodialysis (12–14)	−0.8	0.4
Catalytic gasifier (3, 4, 9, 10)	–	3.5
Syngas expander (4–5)	+10.5	0.7
Syngas compressor (8–9)	−13.9	3.2
SOFC (6–7, 20–21)	+62.3	10.8
Sum	58.3	41.7

In addition to comparing with similarly designed advanced power plants, we also compare the system efficiency of the power plants modeled here with various conventional power plant configurations containing greater than 90% carbon capture and compression of the CO_2 to 15 MPa. Fig. 3 shows the first law system efficiency (Net Work vs. Higher Heating Value, HHV) for a wide range of coal-fired, base-load power plants. The cases in blue are from NETL's analysis of various coal-based power plants [16]; the cases in red are from Li et al. [50]; and the cases in green are for the two configurations analyzed in this section.

As seen in Fig. 3, the system efficiency of a conventional pulverized coal combustion (PCC) power plant with post-combustion carbon capture is around 27%. The system efficiency of an IGCC power plant with pre-combustion carbon capture is between 32% and 43%, depending on (a) the method of oxygen separation from air, (b) the method of separation of CO_2 from H_2, and (c) the temperature of the sulfur removal process. The system efficiency of an IGFC power plant is between 42% and 58%, depending greatly on (a) the type of gasifier, (b) the operating voltage, (c) the pressure of the SOFC, and (d) whether there is anode recycle back to the gasifier. One clear trend in the models is that the system efficiency increases when the carbon dioxide is captured at elevated pressure rather than at atmospheric pressure. Another trend is that system efficiency increases for similar configurations when a catalytic gasifier replaces a conventional entrained flow gasifier. The question we address in the next section of this report is whether the configurations with higher system efficiency are cost effective compared with more traditional PCC-CCS and IGCC–CCS configurations.

3. Economic analysis

3.1. Methodology for economic analysis

While knowing the first or second law efficiency of a power plant is useful in estimating the costs of fueling a power plant, the first or second law efficiency cannot predict the economic viability of the power plant. A detailed knowledge of the capital, fuel and labor costs are required in order to calculate a figure of merit with which to compare the power plant with other investment opportunities. One should not optimize a power plant to obtain maximum system efficiency because the fuel-to-electricity system efficiency does not account for either the cost or the irreversible generation of entropy associated with building, fueling, maintaining, and deconstructing the power plant. Therefore, in addition to the exergy analyses presented earlier, we have also conducted

economic feasibility analyses for these two power plant configurations. The feasibility analyses are Class 4 capital cost estimates as defined by the Association for the Advancement of Cost Engineering International (AACE) [52]. The expected accuracy of a Class 4 capital cost estimate is −15% to −30% on the low side and +20% to +50% on the high side. This means that there will be significant uncertainty in the actual capital cost of the configurations analyzed in this study, and therefore, the capital costs detailed below should be assumed to have the level of uncertain on the order of +50%/−30%.

The goal of this capital cost estimate, as well as the LCOE/IRR analysis, is to evaluate the economic viability of future technologies that have been modeled here, such as H_2 and O_2 separation membranes, catalytic gasifiers, and pressurized SOFCs. Costs for capital, operation and maintenance were determined through cost estimations from the Integrated Environmental Control Model (IECM) [5] for commercial technology and from Gerdes et al. [16,17] for pre-commercial technologies, such as O_2 and H_2 separation membranes. It should be noted that the actual upfront capital cost ($/kW) of PCC and IGCC technologies in recent years has been up to twice the overnight capital cost (2007USD/kW) listed in the papers from which this report has derived its capital cost estimates, and may be due what is called the Averch–Johnson effect [53]. Another reason for this difference may be due to the fact that capital cost values in the literature assume equipment production rates higher than actual production rates. While there is large uncertainty in any large-scale power plant economic analysis, the goal here is simply to help determine whether certain technologies justify further research and development, and should not be construed as support for or against any of companies or technologies discussed above.

One potentially useful economic figure of merit is the levelized cost of electricity (LCOE). The LCOE includes all of the variables related to building, fueling, operating and decommissioning the power plant, and in addition, the LCOE includes the interest rate on the capital loans. A simplified equation for calculating the LCOE is given below:

$$\mathrm{LCOE} = \frac{M + F + P + C \cdot \left[\frac{r(1+r)^n}{(1+r)^n - 1}\right] \cdot (1+r)^t + D \cdot \left[\frac{r}{(1+r)^n - 1}\right]}{E} \tag{9}$$

where M is the yearly operations and maintenance expenditures; F is the yearly fuel expenditures; P is the yearly pollution credit expenditures; C is the upfront capital expenditures; t is the construction time, weighted to account for how funds are spent during start-up; D is the decommissioning investment expenditures; r is the discount/interest rate on the capital loans; n is the number of years the system is operational; and E is the net yearly electricity generation. In this report, we will compare the values of LCOE we calculate with the value of LCOE for other base-load power plants, as calculated by previous studies referenced above. For the LCOE analyses in this report, we use an inflation-adjusted discount rate of 7%/yr. This value was chosen because it is the suggested value for an inflation-adjust discount rate is 7%/yr, according to the US Office of Management and Budget (OMB) [54]. Although, it should be noted that this OMB guideline has not been updated since 1992 and we recognize that the choice of discount rate in an economic analysis should actually reflect the risk of the project and the real rates of return on investment obtained by private or regulated power producers in the same year in which the capital, O&M, and fuel costs were estimated. Since our goal is to evaluate the merits of research and development of new technologies, we have not conducted a risk analysis and we have chosen to use the OMB suggested value of 7%/yr for the real discount rate. To make a fair comparison to other power plant configurations, the fuel price and the discount rate were chosen to be the same in all cases. It should also be noted that, when comparing values of LCOE between different types of power plants, it is important to only compare values of LCOE for projects that produce the same type of electricity output, such as peak-following, base-load, and the various types of intermittent output. Therefore, we only compare the LCOE of the Adv. IGCC–CCS and IFGC–CCS cases with other fossil energy base load power generation plants.

The calculation of the LCOE is significantly more challenging than just the calculation of the system efficiency because, in addition to calculating the system efficiency, one also needs to obtain cost estimates and interest rate estimates. Accurate cost estimates are often hard to find for emerging advanced technologies that have not been broadly commercialized, such as SOFCs, ITMs, and H_2 separation membranes. While there are not many cost estimates for large fuel cell systems, NETL has published some estimates for the capital costs and replacement costs for SOFC systems [16–18,51], for ITM [16], and for H_2 separation [16,55]. It should be noted that the stack costs assume mass production SOFC stacks at the scale of roughly 500 MW installed capacity per year, and therefore the $/kW of stack capital costs used in this and other reports are significantly lower than the $/kW of current SOFC technology.

The other relevant figure of merit used in this paper to compare between power plant configurations is the internal rate of return on investment (IRR). The IRR is the preferred figure of merit when the sale price is known, but the discount rate is uncertain; and it is often the preferred figure of merit when there are two or more products for sale. For example, Larson et al. [56] used an IRR analysis to determine the economic viability of a biomass gasification process in which there were three products for sale: steam, electricity, and liquid biofuels. The average, inflation-adjusted IRR is calculated by determining the rate of return such that the net present value (NPV) of the project equals zero.

$$\mathrm{NPV} = 0 = \sum_{t=1}^{N} \frac{I_t}{(1+i)^t} \tag{10}$$

where I_t is the net income in year t assuming no price/cost inflation, N is the total lifetime of the power plant, and i is the inflation-adjusted rate of return. The IRR is equal to the rate of return earned on the unrecovered balance of the investment. The value of i such that the NPV is equal to zero yields the geometric rate of return on investment for this project, assuming that the yearly income is re-invested in projects with identical rates of return on investment. Hence, for the case of power plants, the IRR measures the exponential nature of growth in the capability to do electrical work [57]. When comparing values of IRR between different types of projects, it is important to only compare values of IRR for projects that are equally risky.

One advantage of an LCOE analysis is that the levelized capital, fuel, and labor cost can be calculated separately and summed together. Another advantage is that the LCOE analysis avoids the self-referential nature of an IRR analysis; this means that the LCOE can never yield multiple solutions. On the other hand, the advantages of an IRR analysis is that it is self-referential, which is important from a public policy perspective because the IRR measures the estimated growth on the capital invested using today's electricity prices and today's capital, labor, and fuel costs. In this report, we calculate both the LCOE (assuming a given real discount rate of 7%) and the IRR (assuming a $50/MWh price of electricity). In subsequent sections, we list the full details behind the LCOE and IRR calculation so that other researchers can use the cost estimates, vary some of the many inputs (fuel price, discount rate, electricity price, etc.), and make economic comparisons with their own power plant designs.

3.2. Economic analysis of IGCC with H_2 and O_2 membranes

We conducted both an IRR and a LCOE analysis of the Adv. IGCC–CCS process described earlier by making assumptions on the capital, fuel and labor costs and then creating cash-flow time-series for the project. The capital and labor costs for the entrained flow gasifier, the gas turbine, the steam turbine, and cooling towers were averaged from the values in the IECM model [5] and those from Gerdes et al. [16,17]. The capital and labor estimates for the non-standard pieces of equipment were taken from a variety of sources, and will be discussed now. The estimated cost of the palladium membranes was \$4800/m^2 of membrane surface area [16]. The estimated cost of the ITM ceramic membranes was \$1500/m^2 of membrane surface area [16]. The amount of area of membranes required was calculated based off the flux of H_2 and O_2 through laboratory scale demonstrations [27,29] of these technologies at the temperatures and pressure differences chosen for the power plant configuration. We estimated a replacement cost of \$8 million and \$10 million every 5 yr for the palladium and ceramic membranes, respectively, based off of the cost and amount of the metals and other materials required to make in the reactor. We estimated that the cost to replace both the H_2 and O_2 membranes is \$22.30/kW every 5 yr. We estimated that H_2S/COS capture using the Paqell process would cost \$174 million, which was based on the cost for commercial Paqell equipment, but at 1/10th the scale [58], assuming a volume scaling factor of 0.8 for costs. The cost assumptions for capital and labor are shown in Table 5 below. These costs include the cost of the equipment plus their share of overhead, i.e. engineering, land, construction, start-up and contingency. The costs associated with the coal handling are included in the gasifier area, and the costs for 50 km of CO_2 pipeline [59] are included in the CO_2 sale/cost section, listed below.

Using the cost assumptions above as well as an average price of base load electricity of \$50/MWh in 2007 USD and fuel price of \$2/GJ for low sulfur, bituminous Appalachian coal, we were able to determine the IRR of the project when the CO_2 was sequestered either into an existing oil–gas well or into a saline reservoir. In the EOR case, we assumed that the CO_2 could be sold at \$15 per metric ton of CO_2 (tCO_2), which is similar to the value of \$12/tCO_2 from Ravagnani et al. [60]. Whereas in the saline aquifer case, we assumed that the owners of the plant would have to pay \$5/tCO_2 to maintain and operate the new wells, which in the middle of the range of prices (\$2–\$7 per metric ton of CO_2) estimated by Eccles et al. [61]. The assumed lifetime of the plant was 25 yr, operating at an 80% capacity factor, and with a 2 yr construction time. The IRR for the EOR case is 8% per year. The IRR for the Saline case is 3% per year.

At an inflation-adjusted discount rate of 7%/yr, the levelized capital costs are \$25/MWh; the maintenance cost are \$14/MWh; and the fuel cost is \$16/MWh. This yields an overall LCOE of \$58/MWh for the saline sequestration case and an overall LCOE of \$47/MWh for enhanced oil recovery. The IRR and the LCOE are both summarized in Table 6, and in addition, we include the uncertainty in the IRR and LCOE due to the +50%/−30% uncertainty in the capital cost of the power plant.

Table 5
Equipment capital costs including its share of overhead. O&M costs included fixed and variable costs, assuming 80% availability. Design power output equals 808 MW. Saline cost equals \$15/tCO_2, and EOR sale price equals \$5/tCO_2, where tCO_2 is metric tons of carbon dioxide generated.

(millions USD 2007)	Initial capital cost	Yearly O&M costs EOR (Saline Seq.)
Air separation unit (ITM)	\$150	\$2
Gasifier area	\$500	\$65
Particulate control	\$10	\$2
Sulfur control	\$170	\$2
WGS and H_2 separation	\$180	\$10
Power block	\$500	\$6
Water treatment	\$20	\$5
Cooling tower	\$100	\$5
CO_2 sale/cost	\$50	−\$54 (\$27)
Total (million \$)	\$1680	\$43 (\$124)
Total (\$/kW)	\$2079	\$53 (\$153)

3.3. Economic analysis of IGFC with catalytic gasifier and pressurized SOFC

The system efficiency calculated earlier for this system was one of many inputs into the economic analysis of this power plant. To do this economic analysis, we assumed a power plant with a net electrical output of 300 MW. In addition to the values of electricity sale price (\$50/MWh) and coal price (\$2/GJ), which are the same as those listed above, some of the major inputs into the economic analysis of this power plant are listed in Table 7. Balance of plant costs were considered to be equal to 25% of total capital costs, and was not included in the Adv. IGCC–CCS configuration modeled previously because the design of the IGCC–CSS is more mature and established.

The non-SOFC capital costs are listed in Table 7 as capital costs divided by the system efficiency because for many of these items, their cost decreases as the system efficiency increases. For example, both the size and cost of the gasifier island decrease as the efficiency of the power plant increases because a smaller gasifier is required to generate the same amount of net power from the plant. The SOFC cost estimates also reflect the increase in price for pressurizing a SOFC. Since to the author's knowledge there are no published estimates of the capital costs of a fluidized bed catalytic gasifier at commercial scale, the capital cost was conservatively assumed to be 50% more expensive than the GE entrained flow gasifier from the previous configuration model when normalized by the same coal flow rate into the gasifier. The capital costs for the various pieces of equipment are listed in Table 8 when the pressure of the SOFC is 0.5 MPa.

The largest capital cost for this system was the SOFC system (\$915 per net kW). Of that cost, 73% is for the stacks, 16% is for the stack enclosures, 8% is for the AC/DC converter, and 3% is for a battery system that can store 4 min of the electricity generated at the power plant. We added the battery to the IGFC system in order to provide a fair comparison with PCC, NGCC, and IGCC systems whose gas and steam turbines can provide spinning reserve for the electrical grid. The second largest cost of the power plant was the gasifier and associated equipment (\$720 per net kW).

Using the cost estimates above and assuming yearly O&M cost estimates equal to 5% of the upfront capital costs, we also examined how the SOFC pressure affects the IRR of this power plant configuration. To do so, we accounted for the change in SOFC voltage as a function of pressure as given Eq. (12). Fig. 4 shows both the exergy efficiency and the IRR of this power plant as a function of the SOFC pressure. The efficiency of the power plant at 2 bar is only roughly 40%, but at 8 bar, the efficiency is roughly 60%. Note that

Table 6
Summary of economic results for Adv. IGCC.

	EOR sequestration	Saline sequestration
IRR at \$50/MWh	8 ± 4 (%/yr)	3 ± 3 (%/yr)
LCOE at 7% real discount rate	47 ± 13 (\$2007/MWh)	58 ± 13 (\$2007/MWh)

Table 7
Capital cost estimates for the Adv. IGFC configuration.

Equipment	Capital cost estimation	Reference
Compressor or expander	\$2536 (Power[kW])$^{0.78}$	Extrapolated from [62]
Heat exchanger	\$1 per cm^2 of cross sectional area required	Extrapolated from [62]
SOFC stack cost	\$1670 per m^2 of active area	Extrapolated from [16,17]
SOFC enclosure	\$80 (p[bar])$^{0.33}$ per kW generated in the SOFC	Extrapolated from [16,17]
SOFC stack replacement	\$175 per kW generated in the SOFC every 5 years	Estimated from [16,17]
Gasifier, solids prep/ handling, and catalyst regeneration	\$420/(System efficiency [%]) per kW of net electricity generated	Extrapolated from [16,17]
50 km CO_2 pipeline	\$60/(System efficiency [%]) per kW of net electricity generated	Estimated from [59]
DC/AC converter	\$70 per kW generated in the SOFC	Estimated from [16,17]
Battery	\$400/kWh of storage	Estimated from [63]

the efficiency is also a strong function of the current density and the air stoichiometric ratio, but we only analyzed the case of current density of 0.5 A cm^{-2} and an air stoichiometric ratio of 2.

As seen in Fig. 4, the value of IRR increases as a function of pressure from 0.2 MPa to 0.8 MPa (2–8 bar); however, after 0.5 MPa, there is minimal increase in the IRR. These diminished returns occur because the increased efficiency with greater pressures is balanced by increased capital costs associated with enclosing and sealing the SOFC at higher pressure. The main reasons why we have presented the breakdown of the capital costs (Table 8) as well as the breakdown of the exergy destruction (Table 4) at a pressure of 0.5 MPa is that there seems to be diminishing returns above 0.5 MPa and this pressure appears to be a reasonably achievable pressure for a SOFC in the near-term because 0.6 MPa is on the high side of pressures tested on the Rolls Royce Fuel Cell System [64]. At a SOFC pressure of 0.5 MPa, the capital cost was \$2600/kW. Due to capital cost uncertainty, a low end of values (\$1800/kW) represents the case in which the assumed gasifier, SOFC, and balance of plant costs have been overestimated, and a high end of values (\$3900/kW) represents the case in which the gasifier, SOFC, and balance of plant costs have been underestimated. Using this range of capital costs and a price of electricity of \$50/MWh, the IRR for the EOR case was 4%/yr ± 4%/yr, and the IRR for the saline aquifer case was 1%/yr ± 4%/yr. Using the range of capital costs and a real discount rate of 7%/yr, the LCOE for the EOR case was 52 ± 17 (\$2007/MWh), and the LCOE for the saline aquifer case was 60 ± 17 (\$2007/MWh), as summarized in Table 9.

Table 8
Capital cost estimate of the power plant shown in Fig. 2. SOFC pressure = 0.5 MPa, SOFC voltage = 0.7 V, SOFC current density = 0.5 A cm^{-2}, gasifier pressure = 3 MPa, system efficiency = 58%.

Capital costs	(\$/kW)
Cathode air compressor	49
Cathode exhaust turbine	51
Syngas expander	42
Syngas compressor	52
CO_2 compressor	17
Gasifier, coal/solid prep, catalyst recovery	720
CO_2 capture and regeneration	120
SOFC, DC/AC converter, and electrical Misc.	915
CO_2 pipelines	100
Balance of plant	517
Total	2583

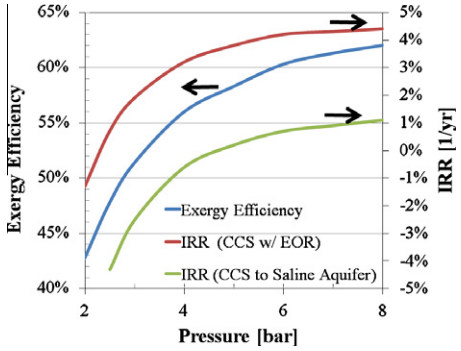

Fig. 4. Exergy efficiency and internal rate of return on investment of the catalytic gasifier w/SOFC modeled in Fig. 2. The current density of the SOFC was 0.5 A cm^{-2}. The air stoichiometric ratio was 2. Red curve is the IRR when the CO_2 is used for enhanced oil recovery, and the green curve is the IRR when the CO_2 is sequestered in a saline aquifer. (For interpretation of the references to color in this figure legend, the reader is referred to the web version of this article.)

4. Discussion and comparison with other economic analyses

4.1. Economic analysis of previous studies

The goal of this section is to present the capital, fuel and labor estimates of various fossil fuel power plant configurations with or without capture of carbon dioxide from previous studies, such as Gerdes et al. [16,17], Grol and Wimer [18], and Rubin et al. [5]. These configurations include pulverized coal combustion (PCC), integrated gasification combined cycle (IGCC), natural gas combined cycle (NGCC), and integrated gasification fuel cell (IGFC). We use capital, fuel and labor estimates from these previous studies, along with fuel prices and a range of possible prices of CO_2 emissions in the near term, to calculate the IRR and LCOE of various power plant configurations. We first present the cost estimates.

Tables 10 and 11 show the first law system efficiency (%), capital costs (2007\$/MWh), construction time (yr), fixed O&M (\$/kW/yr), availability (%), variable O&M (\$/MWh), fuel cost (\$/MWh), and lifetime (yr) of various fossil fuel based power plants. In addition, for the fuel cell systems listed in Table 2, there is a reoccurring cost every 5 yr of \$175/kW of generation due to SOFC stack's replacement. The values of the maintenance/labor costs and fuel costs can be found in Gerdes et al. [16,17], Grol and Wimer [18], and Rubin et al. [5]. All cost and prices estimates in this paper are given in 2007 USD. Using these cost and lifetime estimates, we have generated the inflation-adjusted IRR on investment for all of the major fossil-fuel based power plant configurations, i.e. this is the rate of return on investment assuming that all values of price and cost inflation are exactly equal, as was done in the economic analyses presented earlier in this report.

In Fig. 5, we used the capital and labor estimates listed in Tables 10 and 11 in order to calculate the IRR of various fossil fuel power plants with and without carbon dioxide capture. We assumed a fuel price of \$4/GJ for natural gas and \$2/GJ for coal based off of recent average prices coal and natural gas. As in the earlier economic analyses, we assumed CO_2 is sequestered in saline aquifers at a cost

Table 9
Summary of economic results for the advanced IGFC–CCS configuration at a SOFC pressure of 0.5 MPa, an air stoichiometric ratio of 2.0, and a current density of 0.5 A cm^{-2}.

	EOR sequestration	Saline sequestration
IRR at \$50/MWh	4 ± 4 (%/yr)	1 ± 4 (%/yr)
LCOE at 7% real discount rate	52 ± 17 (\$2007/MWh)	60 ± 17 (\$2007/MWh)

of \$5/tCO$_2$ [61] and assumed CO$_2$ can be sold for EOR at a price of \$15/tCO$_2$ [60]. Fig. 6 shows similar information as Fig. 5, but in Fig. 6, we calculate the LCOE of the various power plant configurations and are able to differentiate between the fuel and CO$_2$ costs, the O&M costs and the levelized capital costs.

Of the power plants analyzed, NGCC power plants yield the highest rate of return on investment. Though, this would only be until the price of CO$_2$ emissions reaches \$25/tCO$_2$. At this price of CO$_2$ emissions, the NGCC power plant would have an IRR of 8%/yr, and this means that the following three different configurations would be equally viable and have an IRR of 8%: NGCC, advanced IGCC–CCS–EOR, and advanced IGFC–CCS–EOR that integrates a catalytic coal gasifier with a pressurized SOFC. The IRR of a conventional IGCC–100%CCS–EOR and the other IGFC configuration would yield an IRR near 6%/yr. Many of the configurations with sequestration in a saline aquifer yield a negative rate of return on investment, including the IGCC–CCS power plant configuration with CO$_2$ sequestration in a saline aquifer. For the configurations with negative values of IRR, this means that more money is spent constructing the facility than is generated in total net yearly revenue. Building a new PCC–CCS power plant configuration is unlikely to be economically viable compared with the alternative options listed above; however, it should be noted that retrofitting existing coal power plants may be economically viable [65], either for carbon capture or for conversion into NGCC power plants.

Since a power plant requires a certain amount of useful physical work to be constructed, fueled, and maintained and since a power plant also generates a certain amount of useful physical work over its lifetime, what we are attempting to express in Fig. 5 is the pretax, inflation-adjusted rate of return on useful physical work invested for various fossil-fuel power plant configurations. Whether these configurations with negative values of IRR, when using an electricity sale price of \$50/MWh, could achieve positive values of IRR at higher sale prices of electricity depends crucially on how much the capital, fuel, and labor costs for these power plants were to increase if the average price of electricity were to increase compared with the price of electricity during the time period that the original capital, fuel and labor costs were estimated. In this study, we chose a value of \$50/MWh (\$2007USD) because it reflects an average base load sale price of electricity to power producers. For example, in 2007 the average price of electricity paid by industrial customers in the US was \$64/MWh, respectively [66]. Since this value of \$64/MWh includes transportation and distribution costs, we have chosen to use the value of \$50/MWh to reflect an average base load sale price of electricity during the time period that the capital, labor, and fuel prices were calculated in this study. If the average price of electricity were to increase in the US, such that \$50/MWh were not an accurate estimate of the sale price of base load electricity, the value of IRR (in units of %/yr) could still remain the same if the percent increase in electricity prices was the same as the percent increase in capital, fuel and labor costs.

We now compare the values of IRR calculated for the Adv. IGCC–CCS and Adv. IGFC–CCS configurations analyzed in detail earlier in this paper to the IRR of the configurations in Fig. 5. The IRR for the Adv. IGCC–CCS–EOR configuration was 8 ± 4 (%/yr) and the IRR for the Adv. IGCC–CCS-Sal.Seq. configuration was 3 ± 3 (%/yr). These values are similar to the values of 8%/yr and 2%/yr, respectively, obtained using lumped cost estimates from Gerdes et al. [16,17] for an IGCC–CCS configuration with H$_2$ and O$_2$ separation membranes and a gas turbine operating solely on hydrogen fuel. The similarity is due to the fact that the designs were quite similar, and the cost estimates for the gasifier and turbines from the IECM are similar to or are the same as the values used by Gerdes et al. [17]. The IRR for the Adv. IGFC–CCS–EOR configuration was 4 ± 4 (%/yr) and the IRR for the Adv. IGFC–CCS–Sal.Seq. configuration was 1 ± 4 (%/yr). These values are similar to the values of 8%/yr and 1%/yr, respectively, obtained using lumped cost estimates by Gerdes

Table 10
Summary of capital, fuel and labor estimates. The capital and labor estimates are from Gerdes et al. [16,17] and Rubin et al. [5]. Fuel prices were assumed to be \$2/GJ for coal and \$4/GJ for natural gas. The assumed inflation-adjusted discount rate is used in the LCOE analysis presented in Figs. 6 and 7. \$ = 2007 USD.

	SC PCC	SC PCC–50%CCS	SC PCC–90%CCS	NGCC	NGCC–90%CCS	Std. IGCC	Std. IGCC–50%CCS	Std. IGCC–90%CCS	IGCC Adv.-95%CCS
HHV efficiency	39.1%	32.9%	27.2%	49.5%	37.8%	38.2%	36.2%	32.5%	40.2%
Capital cost (\$/kW)	1575	2223	2870	600	1200	1813	2102	2390	2169
Weighted construction time (yr)	2	2	2	1	2	2	2	2	2
Fixed O&M (\$/kW/yr)	25	31	37	13	33	35	40	44	44
Availability	85%	80%	80%	85%	80%	80%	80%	80%	80%
Variable O&M (\$/MWh)	4.9	7.1	9.4	3.0	4.0	6.5	7.3	8.1	5.3
Lifetime (yr)	30	30	30	30	30	30	30	30	25
Fuel (\$/MWh)	17.5	20.7	25.1	27.6	36.1	17.9	18.9	21.0	17.0

Table 11
Summary of capital, fuel and labor estimates for SOFC power plants in 2007 USD. The capital and labor estimates for column 1–3 are from Gerdes et al. [16,17]. For comparison, column 4 shows the estimates used Section 3.3 for modeling an advanced IGFC–CCS power plant. Fuel price was assumed to be \$2/GJ for coal. The assumed inflation-adjusted discount rate is used in the LCOE analysis of Fig. 6. \$ = 2007 USD.

	Std Gasifier, 0.1 MPa SOFC	Cat. Gasifier, 0.1 MPa SOFC	Cat. Gasifier, 1.8 MPa SOFC	Cat Gasifier, 0.5 MPa SOFC, anode recycle
HHV efficiency	42%	49%	56%	58%
Capital cost (\$/kW)	2135	2000	1824	2580
Weight construction time (yr)	2	2	2	2
Fixed O&M (\$/kW/yr)	61	68	68	30
Availability	80%	80%	80%	80%
Variable O&M (\$/MWh)	5.0	5.5	5.5	7.6
Plant lifetime (yr)	20	20	20	20
Stack replace time (yr)	5	5	5	5
Stack replacement costs (\$/kW)	175	175	175	175
Fuel (\$/MWh)	16.1	13.9	12.2	11.8

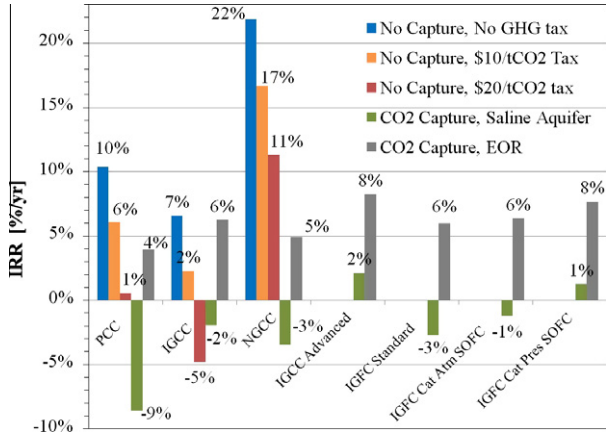

Fig. 5. Internal rate of returns on investment (IRR) of building new fossil fuel, base load power plants. Data in blue represents the rate of return if there is no tax for CO_2 emissions. Data in orange represents the rate of return if there is tax for emissions of \$10/tCO_2. Data in red represents the rate of return if there is tax for emissions of \$20/tCO_2. Data in green represents the rate of return if >90% of the CO_2 is sequestered in saline aquifers at a cost \$5/tCO_2. Data in gray represents the rate of return if >90% of the CO_2 is sold for enhanced oil recovery at a price of \$15/tCO_2. The fuel price for coal was assumed to be \$2/GJ_{th} and the natural gas fuel price was \$4/GJ_{th}. The sale price of electricity was assumed to be \$50/MWh, i.e. \$14/GJ_{el}. \$ = 2007 USD. (For interpretation of the references to color in this figure legend, the reader is referred to the web version of this article.)

et al. [16,17] for an IGFC–CCS configuration with a catalytic gasifier and a pressurized SOFC. Though it should be noted that there were some major differences between the IGFC configuration in Gerdes et al. [16,17] and the one presented here. For example, in the Gerdes et al. [16,17] model there was no anode tail gas recycle and CO_2 capture was accomplished via oxy-combustion of the anode tail gas. In addition, Gerdes et al. [16,17] assumed that the catalytic gasifier costs were same as an entrained flow gasifier when normalized by the flow rate of coal into the gasifier, whereas we assumed that the catalytic gasifier was 50% more expensive per flow rate of coal. This last assumption is one reason why our capital cost estimate of the Adv. IGFC–CCS configuration (\$2583/kW) is higher than the capital cost estimate from Gerdes et al. [16,17] (\$1824/kW), as listed in Table 11.

In Fig. 7, we have separated out those power plants configurations shown in Fig. 6 that have a value of LCOE of roughly \$50/MWh or less at a real discount of 7%/yr and that meet the EPA's proposed rule of 0.45 kg (1 lb) of CO_2 per kWh of electricity generated [2], which was released on March 27, 2012. These configurations, in order of least cost to highest cost, are NGCC, Adv. IGCC–100%CCS–EOR, IGCC–50%CCS–EOR, Adv. IGFC–100%CCS–EOR (18 bar SOFC), PCC–50%CCS–EOR, NGCC–100%CCS–EOR, Std. IGCC–100%CCS–EOR, and Adv. IGFC–100%CCS–EOR (1 bar SOFC). At a price of natural gas of \$4/GJ, the NGCC configuration has the lowest price of electricity. At a price of natural gas near \$6/GJ, the LCOE of the NGCC power plant will be equal to the LCOE of the Adv. IGCC–100%CCS–EOR configuration. It should be noted that we have not analyzed any power plant retrofit configurations, and therefore, the conclusions listed above only pertain to the economics of building new power plant constructions. In the next section, we analyze the case of varying both the prices of natural gas and the prices of CO_2 emissions.

4.2. Varying the price of natural gas and CO_2 emissions

The results presented in Fig. 5 suggest that the IRR of an advanced IGCC–CCS power plant is similar to the IRR of an advanced IGFC–CCS if the catalytic gasifier costs are the similar to the cost of an entrained flow gasifier for similar input of coal and if SOFC technology can achieve mass production cost targets. However, the values of IRR calculated for these advanced power plant configurations were well below the IRR of a NGCC power plant with today's fuel prices and no CO_2 tax. We now address the following question: at what price of natural gas and at what price of CO_2 emissions would an advanced IGCC–CCS–EOR or IGFC–CCS–EOR power plant configuration be economically viable? We therefore conducted an LCOE analysis for the various power plant configurations as a function of the price of natural gas and carbon dioxide emissions, holding all other variables constant.

Figs. 8 and 9 show which fossil fuel power plant configuration has the lowest LCOE as a function of the cost of natural gas (NG) and the cost of emitting CO_2 into the atmosphere while holding the cost of coal at \$2/GJ. In Fig. 8, we assume that the captured

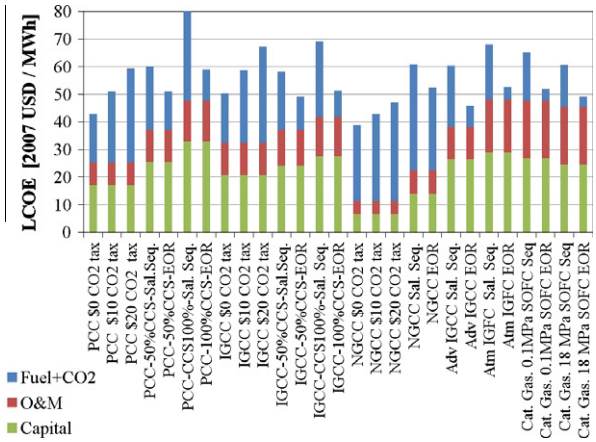

Fig. 6. Levelized cost of electricity (LCOE) in 2007 USD/MWh of building new fossil fuel, base load power plants. The cost is broken down into levelized capital costs, the fixed plus variable O&M, and the sum of the cost for fuel plus CO_2 emissions or sales. 'Sal. Seq.' means sequestration in saline aquifers at a cost \$5/tCO_2. 'EOR' means enhanced oil recovery at a positive sale price of \$15/tCO_2. The fuel price for coal was assumed to be \$2/GJ_{th} and the natural gas fuel price was \$4/GJ_{th}. The assumed inflation-adjusted discount rate was 7%/yr. Capital and O&M cost estimates are listed in Tables 1 and 2.

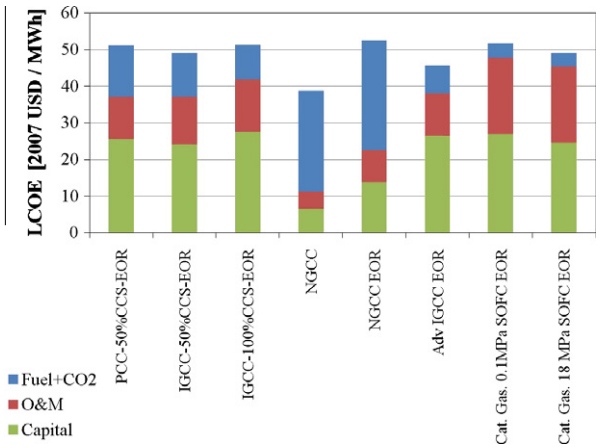

Fig. 7. Levelized cost of electricity (LCOE) in 2007 USD/MWh of building new fossil fuel, base load power plants. The configurations above meet proposed EPA regulations of 0.45 kg (1 lb) of CO_2 per kWh of electricity generated. The cost is broken down into levelized capital costs, the fixed plus variable O&M, and the sum of the cost for fuel plus CO_2 EOR sales at \$15/tCO_2. The fuel price for coal was assumed to be \$2/GJ_{th} and the natural gas fuel price was \$4/GJ_{th}. The assumed inflation-adjusted discount rate was 7%/yr. Capital and O&M cost estimates are listed in Tables 1 and 2.

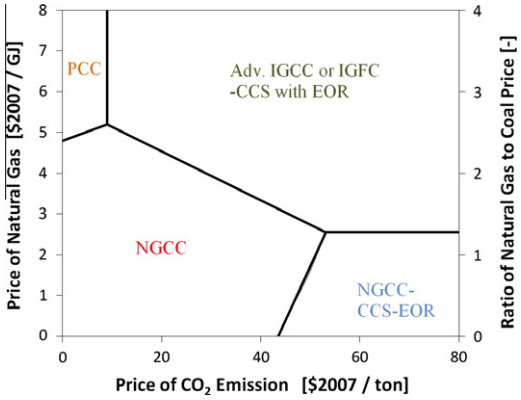

Fig. 8. The lowest cost of electricity between PCC, NGCC, NGCC–CCS–EOR, Adv. IGFC–CCS–EOR, and Adv. IGCC–CCS–EOR, as a function of the price of natural gas and CO_2 emissions, assuming an EOR sale price of \$15/ton of CO_2, using cost estimates from Gerdes et al. [16,17]. The price of coal was held constant at \$2/GJ in 2007USD.

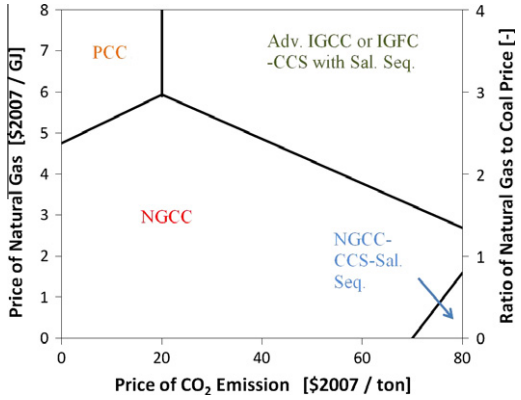

Fig. 9. The lowest cost of electricity between PCC, NGCC, NGCC–CCS-SalSeq, Adv. IGFC–CCS-SalSeq, and Adv. IGCC–CCS-SalSeq, as a function of the price of natural gas and CO_2 emissions, assuming a Saline Sequestration cost of \$5/ton of CO_2, using cost estimates from Gerdes et al. [16,17]. The price of coal was held constant at \$2/GJ in 2007USD.

CO_2 can be used for EOR, whereas in Fig. 9, we assume that the captured CO_2 must be sequestered in a saline aquifer. For the EOR case, we found that if the price of natural gas goes above the line between the points (\$10/tCO_2, \$5.0/GJ) and (\$50/tCO_2, \$2.5/GJ), then the Adv IGCC & IGFC–CCS–EOR configurations have the lowest levelized cost of electricity. Note also that there is line at which a NGCC–CCS power plant has the lowest value of LCOE and there is also a vertical line around \$10/tCO_2 at which a PCC has the lowest value of LCOE. There is also a horizontal line just below \$2.5/GJ, which shows when the Adv. IGCC and IGFC–CCS configurations and NGCC–CCS configurations have the same LCOE. For saline sequestration (ca. Fig. 9), the area in the graph in which NGCC has the lowest value of LCOE increases substantially. The results in Fig. 8 are fairly similar to the results presented in Fig. 3 of Fischbeck et al. [12], who present a case in which captured carbon dioxide is assumed to obtain a sale price of \$25/tCO_2. However, one major difference is that our 'Coal with CCS' case was an Adv. IGCC–CCS configuration rather than a PC–CCS configuration.

The economic analyses conducted here suggest that there might be scenarios in which Adv IGCC and IGFC–CCS power plant configurations are economically preferable; however, this requires either an increase in the price of natural gas or an increase in the price of CO_2 emissions. It should also be noted that this analysis held the price of capital, labor, and coal constant while varying the price of natural gas and the price of CO_2 emission. The price of capital, labor, and coal is unlikely to remain constant with changing price of natural gas and CO_2 emission, so the conclusion we drawn from these figures should not be used as predictions for future outcomes. Instead, they should be used to determine which power plant configurations deserve further research and development. It should be noted that the advanced IGCC and IGFC configuration studied here still require significant levels of research and development before they are commercially-viable for large scale power plants. Specifically, this means scaling up H_2 and O_2 membrane technology, further testing operation of gas turbines on hydrogen, scaling up the size of the catalytic gasifier, proving the catalyst regeneration process, and scaling up the size and pressure of SOFCs.

5. Conclusions

We conducted exergy and economic analyses for two advanced coal-based power plants with CO_2 capture and sequestration. When conducting our capital cost analysis for the advanced IGCC–CCS–EOR design, we calculated a system efficiency of 43% and a value of IRR of 8 ± 4%/yr (at \$50/MWh), which was similar to the value estimated in previous studies [16,17]. When conducting our capital cost analysis for the advanced IGFC–CCS–EOR design, we calculated a system efficiency of 58% and a value of IRR of 4 ± 4%/yr (at \$50/MWh), which was also close to the values estimated by previous researchers. We used capital and labor cost estimates from previous researchers in order to compare the IRR of these two advanced power plant designs with conventional and other advanced power plant designs. Using cost estimates from other studies and assuming recent fuel and electricity prices, a natural gas combined cycle (NGCC) power plant yielded the highest value of rate of return on investment (22%/yr). However, our results suggest that, in the case of a CO_2 tax of \$25/tCO_2, then three different configurations are equally viable economically (IRR = 8%/yr at \$50/MWh): a NGCC power plant without capture, an advanced IGCC–CCS–EOR power plant with H_2 and O_2 membranes, and an advanced IGFC–CCS–EOR power plant that integrates a catalytic coal gasifier with a pressurized SOFC.

This research suggests that there may be advanced coal-based power plants that can achieve reasonable values of IRR (8%/yr) at today's typical prices for base load electricity generation of \$50/MWh; and therefore, research into advanced H_2 and O_2 separation membranes as well as pressurized SOFCs are of crucial importance to the development of low cost base load electricity if the price of natural gas in the future goes above \$5/GJ and the price of CO_2 emissions goes above \$20/tCO_2. The calculations in this report suggest that there may be scenarios in which advanced IGCC and IGFC configuration are economically viable, meriting further research and development into these technologies.

Acknowledgments

We thank Dhruv Bhatnagar and Srikant Subramaniam for their contributions to this work. We thank Drs. Jay Apt, David Berry, Phil DiPietro, Paul Fischbeck, Kristin Gerdes, Dale Keairns, David Rode, Edward Rubin, Dushyant Shekhawat, Wayne Surdoval, and Jan Thijssen for their discussions on this topic. We thank the financial support of the National Energy Technology Laboratory as part of the US Department of Energy.

References

[1] US Department of Energy, Energy Information Administration, International Energy, Outlook 2006, DOE/EIA-0484; 2006.
[2] EPA-HQ-OAR-2011-0660; FRL-RIN 2060-AQ91. Standards of performance for greenhouse gas emissions for new stationary sources.

[3] Herzog HJ. The economics of CO_2 capture. Greenhouse gas control technologies; 1999. p. 101–6.
[4] Johnson TL, Keith DW. Fossil electricity and CO_2 sequestration: how natural gas prices, initial conditions and retrofits determine the cost of controlling CO_2 emissions. Energy Policy 2004;32(3):367–82.
[5] Rubin ES, Chen C, Rao AB. Cost and performance of fossil fuel power plants with CO_2 capture and storage. Energy Policy 2007;35(9):4444–54.
[6] Rubin ES, Mantripragada H, Marks A, Versteeg P, Kitchin J. The outlook for improved carbon capture technology. Progr Energy Combust 2012;38(5): 630–71.
[7] Davison J. Performance and costs of power plants with capture and storage of CO_2. Energy 2007;32(7):1163–76.
[8] Patino-Echeverri D, Fischbeck P, Kriegler E. Economic and environmental costs of regulatory uncertainty for coal-fired power plants. Environ Sci Technol 2009;43(3):578–84.
[9] Kunze C, Spliethoff H. Modelling of an IGCC plant with carbon capture for 2020. Fuel Process Technol 2010;91(8):934–41.
[10] Hu Y, Li H, Yan J. Techno-economic evaluation of the evaporative gas turbine cycle with different CO_2 capture options. Appl Energy 2012;89(1):303–14.
[11] Hammond GP, Akwe SSO, Williams S. Techno-economic appraisal of fossil-fuelled power generation systems with carbon dioxide capture and storage. Energy 2011;36(2):975–84.
[12] Fischbeck PS, Gerard D, Mccoy ST. Sensitivity analysis of the build decision for carbon capture and sequestration projects. Greenhouse Gases: Sci Technol 2012;2(1):36–45.
[13] Viebahn P, Daniel V, Samuel H. Integrated assessment of carbon capture and storage (CCS) in the German power sector and comparison with the deployment of renewable energies. Appl Energy 2012;97:238–48.
[14] Pettinau A, Ferrara F, Amorino C. Techno-economic comparison between different technologies for a CCS power generation plant integrated with a sub-bituminous coal mine in Italy. Appl Energy 2012;99:32–9.
[15] Melchior T, Madlener R. Economic evaluation of IGCC plants with hot gas cleaning. Appl Energy 2012;97:170–84.
[16] Gerdes K. Current and future technologies for gasification-based power generation. A pathway study focused on carbon capture advanced power systems R&D using bituminous coal, DOE/NETL-2009/1389, vol. 2; 2010.
[17] Gerdes K, Grol E, Keairns D, Newby R. Integrated gasification fuel cell performance and cost assessment: Doe/Netl-2009/1361; 2009.
[18] Grol E, Wimer J. Systems analysis of an integrated gasification fuel cell combined cycle: Doe/Netl- 40/080609; 2009.
[19] Li M, Rao AD, Samuelsen GS. Performance and costs of advanced sustainable central power plants with CCS and H(2) co-production. Appl Energy 2012;91(1):43–50.
[20] Chen C, Rubin ES. CO_2 control technology effects on IGCC plant performance and cost. Energy Policy 2009;37(3):915–24.
[21] Elsayed YM, Evans RB. Thermoeconomics and design of heat systems. J Eng Power 1970;92(1). 27–&.
[22] El-Sayed Y. The thermoeconomics of energy conversions. Elsevier; 2003.
[23] Bejan A. Entropy generation minimization: the method of thermodynamic optimization of finite-size systems and finite-time processes. CRC Press; 1996.
[24] Lu GQ, Da Costa JCD, Duke M, Giessler S, Socolow R, Williams RH, et al. Inorganic membranes for hydrogen production and purification: a critical review and perspective. J Colloid Interf Sci 2007;314(2):589–603.
[25] Kulprathipanja A, Alptekin GO, Falconer JL, Way JD. Pd and Pd–Cu membranes: inhibition of H-2 permeation by H_2S. J Membr Sci 2005;254(1–2):49–62.
[26] Ku AY, Kulkarni P, Shisler R, Wei W. Membrane performance requirements for carbon dioxide capture using hydrogen-selective membranes in integrated gasification combined cycle (IGCC) power plants. J Membr Sci 2011;367(1–2): 233–9.
[27] Morreale BD, Ciocco MV, Enick RM, Morsi BI, Howard BH, Cugini AV, et al. The permeability of hydrogen in bulk palladium at elevated temperatures and pressures. J Membr Sci 2003;212(1–2):87–97.
[28] Mancini ND, Mitsos A. Ion transport membrane reactors for oxy-combustion – Part I: intermediate-fidelity modeling. Energy 2011;36(8):4701–20.
[29] Sunarso J, Baumann S, Serra JM, Meulenberg WA, Liu S, Lin YS, et al. Mixed ionic–electronic conducting (MIEC) ceramic-based membranes for oxygen separation. J Membr Sci 2008;320(1–2):13–41.
[30] Hirsch RL, Gallagher JE, Lessard RR, Wesselhoft RD. Catalytic coal-gasification – an emerging technology. Science 1982;215(4529):121–7.
[31] Nahas NC. Exxon catalytic coal-gasification process – fundamentals to flowsheets. Fuel 1983;62(2):239–41.
[32] Espinal JF, Mondragon F, Truong TN. Mechanisms for methane and ethane formation in the reaction of hydrogen with carbonaceous materials. Carbon 2005;43(9):1820–7.
[33] Siefert N, Shekhawat D, Litster S, Berry D. Molten catalytic coal gasification with in situ carbon and sulphur capture. Energy Environ Sci 2012;5(9): 8660–72.
[34] Yeboah YD, Xu Y, Sheth A, Godavarty A, Agrawal PK. Catalytic gasification of coal using eutectic salts: identification of eutectics. Carbon 2003;41(2): 203–14.
[35] Sheth A, Yeboah YD, Godavarty A, Xu Y, Agrawal PK. Catalytic gasification of coal using eutectic salts: reaction kinetics with binary and ternary eutectic catalysts. Fuel 2003;82(3):305–17.
[36] Leonhardt P, Sulimma A, Van Heek K-H, Jüntgen H. Steam gasification of German hard coal using alkaline catalysts: effects of carbon burn-off and ash content. Fuel 1983;62(2):200–4.
[37] Nagasawa H, Yamasaki A, Iizuka A, Kumagai K, Yanagisawa Y. A new recovery process of carbon dioxide from alkaline carbonate solution via electrodialysis. AIChE J 2009;55(12):3286–93.
[38] Merkel TC, Zhou MJ, Baker RW. Carbon dioxide capture with membranes at an IGCC power plant. J Membr Sci 2012;389:441–50.
[39] Blamey J, Anthony EJ, Wang J, Fennell PS. the calcium looping cycle for large-scale CO_2 capture. Progr Energy Combust 2010;36(2):260–79.
[40] Ohrn T, Liu Z. Rolls-Royce Coal-Based SECA Program Update. In: 12th Annual Seca Conference, Pittsburgh, Pa, July 2011.
[41] Zhang LM, Cong Y, Yang WS, Lin LW. A direct ammonia tubular solid oxide fuel cell. Chin J Catal 2007;28(9):749–51.
[42] Ma QL, Ma JJ, Zhou S, Yan RQ, Gao JF, Meng GY. A high-performance ammonia-fueled SOFC based on a YSZ thin-film electrolyte. J Power Sources 2007;164(1):86–9.
[43] Farhad S, Yoo Y, Hamdullahpur F. Effects of fuel processing methods on industrial scale biogas-fuelled solid oxide fuel cell system for operating in wastewater treatment plants. J Power Sources 2010;195(5):1446–53.
[44] Lanzini A, Leone P. Experimental investigation of direct internal reforming of biogas in solid oxide fuel cells. Int J Hydrogen Energy 2010;35(6): 2463–76.
[45] Shiratori Y, Ijichi T, Oshima T, Sasaki K. Internal reforming SOFC running on biogas. Int J Hydrogen Energy 2010;35(15):7905–12.
[46] Shiratori Y, Oshima T, Sasaki K. Feasibility of direct-biogas SOFC. Int J Hydrogen Energ 2008;33(21):6316–21.
[47] Laycock CJ, Staniforth JZ, Ormerod RM. Biogas as a fuel for solid oxide fuel cells and synthesis gas production: effects of ceria-doping and hydrogen sulfide on the performance of nickel-based anode materials. Dalton Trans 2011;40(20): 5494–504.
[48] Yang L, Wang SZ, Blinn K, Liu MF, Liu Z, Cheng Z, et al. Enhanced sulfur and coking tolerance of a mixed ion conductor for SOFCS: Bazr0.1ce0.7y0.2-Xybxo3-delta. Science 2009;326(5949):126–9.
[49] Cheng Z, Wang JH, Choi YM, Yang L, Lin MC, Liu ML. From Ni–YSZ to sulfur-tolerant anode materials for SOFCS: electrochemical behavior, in situ characterization, modeling, and future perspectives. Energy Environ Sci 2011;4(11):4380–409.
[50] Li M, Rao AD, Brouwer J, Samuelsen GS. Design of highly efficient coal-based integrated gasification fuel cell power plants. J Power Sources 2010;195(17):5707–18.
[51] Shelton W. Analysis of integrated gasification fuel cell plant configurations, DOE/NETL-2011-1482; 2011.
[52] Prichett MB, Griesmyer PW, Mcdonald DF, Venters VG, Dysert LR. AACE international certified cost technician primer. AACE International, Inc.; 2011.
[53] Averch H, Johnson L. The behavior of the firm under regulatory constraint. Am. Econ. Rev. 1962;52(5):1052–69.
[54] Office of Management and Budget. Circular No. A-94 Revised. Guidelines and Discount Rates for Benefit-Cost Analysis of Federal Programs, October 29, 1992. <http://Www.Whitehouse.Gov/Omb/Circulars_A094> [Cited September 8, 2012, About 12 Screens].
[55] Gerdes K. Production of high purity hydrogen from domestic coal: assessing the techno-economic impact of emerging technologies, DOE/NETL-2010/1432; 2010.
[56] Larson ED, Consonni S, Katofsky RE, Iisa K, Frederick WJ. An assessment of gasification-based biorefining at Kraft pulp and paper mills in the United States, Part B: results. Tappi J 2009;8(1):27–35.
[57] Warr B, Ayres RU. Useful work and information as drivers of economic growth. Ecol Econ 2012;73:93–102.
[58] Cline C, Hoksber A, Abry R, Janssen A. Biological process for H_2S removal from gas streams. The shell-paques/Thiopaq gas desulfurization process. LRGCC, Norman, Oklahoma, February 2003.
[59] Mccoy ST, Rubin ES. An engineering-economic model of pipeline transport of CO_2 with application to carbon capture and storage. Int J Greenhouse Gas Control 2008;2(2):219–29.
[60] Ravagnani ATFSG, Ligero EL, Suslick SB. CO_2 sequestration through enhanced oil recovery in a mature oil field. J Petrol Sci Eng 2009;65(3–4):129–38.
[61] Eccles JK, Pratson L, Newell RG, Jackson RB. Physical and economic potential of geological Co(2) storage in saline aquifers. Environ Sci Technol 2009;43(6): 1962–9.
[62] Silla H. Chemical process engineering: design and economics. M. Dekker; 2003.
[63] Sundararagavan S, Baker E. Evaluating energy storage technologies for wind power integration. Sol Energy 2012;86(9):2707–17.
[64] Ohrn T, Liu Z. Rolls-Royce coal-based SECA program update, 2011 SECA conference; 2011.
[65] Eppink J, Marquis M, Nichols C. Coal-fired power plants in the United States: examination of the costs of retrofitting with CO_2 capture technology, revision 3, DOE/NETL-402/102309; 2011.
[66] US Electricity Information Administration, A. P. B. S. B. P., Eia-861, January 2012. <http://Www.Eia.Gov/Electricity/Data/State/>.